

# A Water-Soluble Hybrid Material of Single-Walled Carbon Nanotubes with an Amphiphilic Poly(phenyleneethynylene): Preparation, Characterization, and Photovoltaic Properties

Jie Mao<sup>1</sup>, Qian Liu<sup>2</sup>, Xin Lv<sup>1</sup>, Zunfeng Liu<sup>1</sup>, Yi Huang<sup>1</sup>, Yanfeng Ma<sup>1</sup>,  
Yongsheng Chen<sup>1,\*</sup>, and Shougen Yin<sup>2,\*</sup>

<sup>1</sup>Key Laboratory for Functional Polymer Materials and Center for Nanoscale Science and Technology,  
Institute of Polymer Chemistry, College of Chemistry, Nankai University, Tianjin 300071, China

<sup>2</sup>Institute of Material Physics, Tianjin University of Technology, Tianjin 300191, China

A novel rigid linear polymer poly(phenyleneethynylene) (PPE) was synthesized and the polymer exhibits good solubility in both water and common organic solvents. The interaction at both ground and excited state between this polymer and single-walled carbon nanotubes (SWNTs) was studied and a water-soluble nano-scale PPE/SWNTs hybrid was fabricated, where the water solubility of SWNTs was enhanced to 1.8 mg/ml. Steady state fluorescence spectra and fluorescence lifetime decay measurements showed that the emissions from PPEs in this hybrid at excited state were efficiently quenched by the attachment of SWNTs, where an efficient energy transfer happened from PPEs to SWNTs as the electron acceptor. Using this hybrid as the active layer we fabricated a photovoltaic cell with the bulk heterojunction configuration, and it showed a photoresponse with an open circuit voltage ( $V_{oc}$ ) of 105 mV and a short circuit current density ( $I_{sc}$ ) of 28.7  $\mu\text{A}/\text{cm}^2$  under standard AM 1.5 illumination (100  $\text{mW}/\text{cm}^2$ ).

**Keywords:** Single-Walled Carbon Nanotubes, Non-Covalent Functionalization, Energy Transfer, Photovoltaic Cell, Poly(phenyleneethynylene).

## 1. INTRODUCTION

Single-walled carbon nanotubes (SWNTs) are one of the most striking discoveries in chemistry and materials science recently. Their remarkable physical and chemical properties have made this material a much attractive candidate for many structural and electronic applications.<sup>1–5</sup> However, challenges still remain before many of these prospects could be materialized. In particular, two of these challenges for bulk applications include (1) removing the impurities inherited from the nanotube synthesis and (2) well-dispersing these tubes in solvents or matrix, preferably as individual or small bundles of SWNTs. As most of the purification methods for SWNTs unavoidably add hydroxyl or carboxyl groups on the surface of SWNTs, which make them much more hydrophilic, it would be obvious and environmentally friendly to process SWNTs using water. Poly(phenyleneethynylene)s (PPEs) are a class of rigid-rod conjugated polymers composed

of aromatic rings and alkyne functional groups and have been reported to form  $\pi$ - $\pi$  stacking hybrid with SWNTs.<sup>6</sup> They are of great interest because of their semiconductor-like properties and ease of processing, which make them fulfill the requirements for many applications especially in electronic and photonic devices.<sup>7</sup> However, very few researches about PPE/SWNTs system have been reported since the discovery of carbon nanotubes in 1991.<sup>6</sup> The findings of recent research reveal that PPEs exhibit promising photovoltaic properties when they are fabricated with  $C_{60}$ , and PPEs act as an “antenna” to harvest optical energy and transfer it to the acceptor unit,  $C_{60}$ .<sup>8–10</sup> Comparing with  $C_{60}$ , SWNTs have much advantage in electron transfer properties because of their huge  $\pi$ - $\pi$  conjugation and one-dimensional structure. Recently, some well-characterized  $\pi$ -conjugated molecules have been widely used to modify carbon nanotubes, which represents an emerging strategy in developing nanoscale photoactive materials especially for photovoltaic applications.<sup>4</sup> For example, Kymakis and Amaratunga et al. used a  $\pi$ -conjugated polymer, poly(3-octylthiophene), and SWNTs

\*Authors to whom correspondence should be addressed.

to construct photoactive materials, which was fabricated into photovoltaic devices showing the property of converting light energy into electric power.<sup>11–13</sup> Mcleskey et al. found that the environmentally friendly hybrid material of a water-soluble polythiophene with SWNTs exhibited photoresponse and the potential for use in photovoltaics.<sup>14</sup> In these polymeric photovoltaic (PV) devices, a bulk donor–acceptor heterojunction is formed to enhance the efficiency of excitons generation, dissociation, and charge transportation for better PV performance. All these polymer/SWNTs systems exhibited enhanced photoactive properties comparing with their parent materials without carbon nanotubes.<sup>4, 11–13, 15</sup> But well-dispersion of SWNTs in the polymer matrix still remains to be improved for better PV performance. In our earlier work<sup>16, 17</sup> and other results,<sup>4</sup> it has been found that SWNTs can efficiently transfer light energy as the electron acceptor with chromophore molecules. Thus using a water-soluble PPE, we can not only be able to dissolve/process SWNTs but also make nano-scale hybrid materials in aqueous medium to take advantage of the excellent properties of both PPEs and SWNTs for multifunctional purposes. Particularly, it enables us to tailor their properties while still preserving nearly all of the intrinsic nanotube's properties due to the non-covalent functionalization.

Herein, we use a water-soluble PPE as the hybridizing agent for SWNTs to construct a novel hybrid structure PPE/SWNTs (Fig. 1) and a variety of spectroscopy measurements were employed to characterize the interactions between PPEs and SWNTs. The results show that strong interaction exists between PPEs and SWNTs, which enhances the water solubility of SWNTs up to 1.8 mg/ml. Furthermore, at the excited state an efficient energy transfer happens from PPEs to SWNTs. Thus as our first device application based on these results, we have fabricated a photovoltaic cell using the bulk heterojunction concept based on this hybrid material and examined its photovoltaic properties. The results show such PPE/SWNTs nano-hybrids are promising light energy conversion materials.

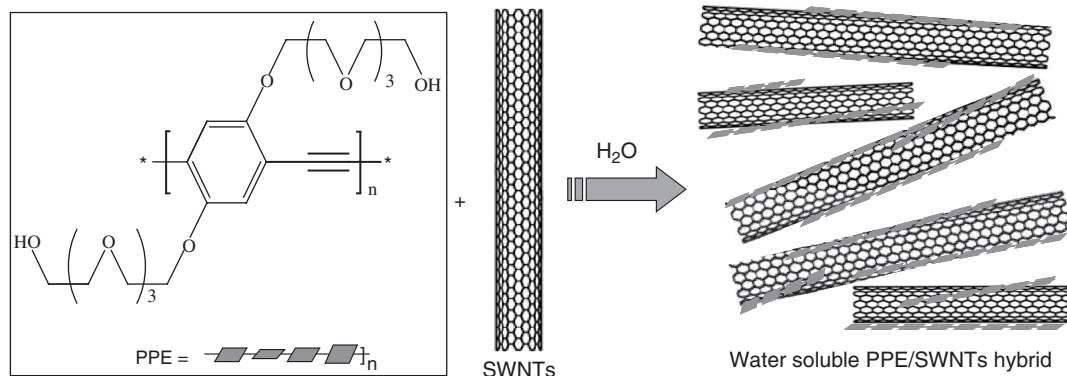


**Fig. 1.** Schematic view for the supramolecular assembly of the conjugated polymer PPE with SWNTs, forming a water-soluble PPE/SWNTs hybrid.

## 2. EXPERIMENTAL DETAILS

### 2.1. Materials

The SWNTs were prepared by our direct current arc-discharge method.<sup>18</sup> All chemical reagents used in this study were purchased from commercial sources (Alfa, Acros, and Aldrich). Toluene was purified by distillation from sodium in the presence of benzophenone. Other organic solvents were used without any further purification. 1,4-Diiodo-2,5-bis(11-hydroxyl-3,6,9-trioxaundecyl)-benzene (monomer 1) was synthesized according to the literature procedures.<sup>19</sup> Indium tin oxide (ITO) coated glass,  $R_s = 15 \sim 30 \Omega \text{ square}^{-1}$ , was purchased from CSG Inc. All reactions were carried under argon if not stated otherwise.

### 2.2. Instruments and Measurements

UV-Vis-NIR spectra were obtained with a JASCO V-570 spectrometer. Fluorescence spectra were obtained with FluoroMax-P. Fluorescence lifetimes were obtained on a FL920 fluorescence lifetime spectrometer (Edinburgh Instruments) by using the time-correlated single-photon counting method. <sup>1</sup>H NMR spectra were recorded on a Bruker (300 MHz) spectrometer using TMS as the internal standard. Gel permeation chromatography (GPC) analysis was conducted on a Waters 510 system using polystyrene as standard and THF as eluent. Transmission electron microscope (TEM) images were obtained on a FEI TECNAI-20 instrument operated at 200 kV. Atomic force microscopy (AFM) images were obtained on a Nanoscope IV (Digital Instruments Inc.) using the tapping mode. Centrifugation was carried out with an Eppendorf 5810R centrifuge. The current–voltage ( $I$ – $V$ ) measurement of the photovoltaic devices was conducted on a computer controlled Keithley 2400 Source Measure Unit. A Xenon lamp with AM 1.5 filter was used as the white light source, and the optical power at the sample was  $100 \text{ mW/cm}^2$ .

## 2.3. Synthesis of Poly((2,5-bis(11-hydroxy-3,6,9-trioxaundecyl)-p-phenylene)ethynylene) (Scheme 1)

### 2.3.1. 1,4-Diethynyl-2,5-bis(11-hydroxy-3,6,9-trioxaundecyl)benzene (monomer 2)

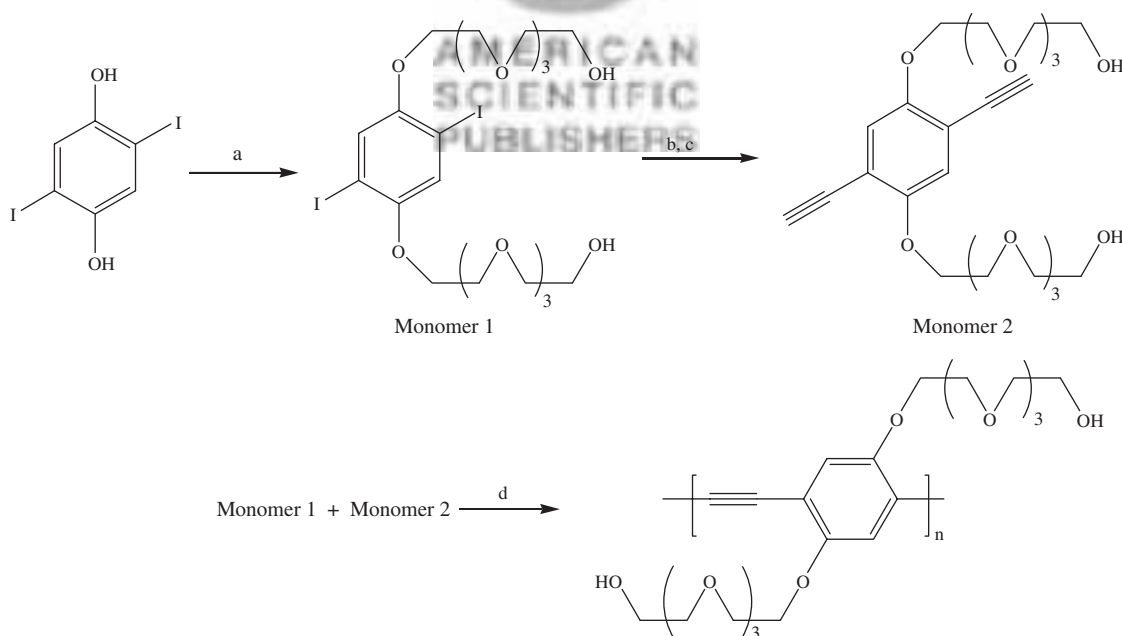
1,4-Diiodo-2,5-bis(11-hydroxy-3,6,9-trioxaundecyl)benzene (1.35 g, 1.9 mmol) was combined with *trans*-dichlorobis(triphenylphosphine)palladium (II) (34.6 mg, 57  $\mu$ mol, 0.03 eq) and copper (I) iodide (23.1 mg, 114  $\mu$ mol, 0.06 eq) in a dried flask equipped with a stir bar. The flask was evacuated and refilled with argon three times. The solids were dissolved/suspended in toluene (30 ml) and diisopropylamine (DIPA) (3 ml). (Trimethylsilyl)acetylene (0.60 ml, 4.2 mmol, 2.2 eq) was then added, and the reaction was stirred and heated to 60 °C for 22 h. Once the reaction was cooled to room temperature, saturated ammonium chloride solution was added. After the mixture was stirred further for 30 min, ether (~50 ml) was added. The separated organic layer was washed four times with saturated ammonium chloride solution, dried with magnesium sulfate, filtered, and concentrated to give dark brown oil. Then the crude product was chromatographed on silica gel (ethyl acetate) to give 1,4-bis(trimethylsilylacetylene)-2,5-bis(11-hydroxy-3,6,9-trioxaundecyl)benzene (1.20 g, 1.83 mmol, 96%).  $^1\text{H NMR}$  (300 MHz,  $\text{CDCl}_3$ ):  $\delta$  0.246 (s, 18H), 3.59–3.62 (m, 4H), 3.68–3.73 (m, 16H), 3.78–3.81 (m, 4H), 3.88 (t, 4H,  $J = 4.8$  Hz), 4.09–4.16 (m, 4H), 6.92 (s, 2H).

The bistrimethylsilylacetylene (1.18 g, 1.80 mmol, 1 eq) from above was de-protected by reaction with aqueous

potassium hydroxide (200 mg, 3.6 mmol, 2 eq; dissolved in 1 ml of DDI water) in degassed THF (17 ml) and methanol (13 ml) under an argon atmosphere. The solution was stirred for 48 h. The reaction was then poured into 50 ml of ether. The organic layer was separated and washed with water three times, dried with magnesium sulfate and concentrated to give a brown oil which was chromatographed on silica gel (methanol/ethyl acetate 1/8) to yield 1,4-diethynyl-2,5-bis(11-hydroxy-3,6,9-trioxaundecyl)benzene (monomer 2).  $^1\text{H NMR}$  (300 MHz,  $\text{CDCl}_3$ ):  $\delta$  2.21 (br s, 2H), 3.35 (s, 2H), 3.61 (m, 4H), 3.70 (m, 16H), 3.77 (m, 4H), 3.87 (t, 4H,  $J = 4.8$  Hz), 4.16 (m, 4H), 7.00 (s, 2H). ESI-MS: 533.68 ( $\text{M} + \text{H}^+$ ).

### 2.3.2. Poly((2,5-bis(11-hydroxy-3,6,9-trioxaundecyl)-p-phenylene)ethynylene) (PPE)

A 25 ml Schlenk flask equipped with a stir bar was charged with 1,4-diethynyl-2,5-bis(11-hydroxy-3,6,9-trioxaundecyl)benzene (60 mg, 0.118 mmol, 1.05 eq) and 1,4-diiodo-2,5-bis(11-hydroxy-3,6,9-trioxaundecyl)benzene (80 mg, 0.112 mmol, 1 eq). Tetrakis-(triphenylphosphine)palladium (0) (6.5 mg, 5.6  $\mu$ mol, 0.05 eq) and copper(I) iodide (2.0 mg) were added to the flask under an argon atmosphere. The flask was degassed by three freeze-pump-thaw cycles after adding Toluene (10 ml) and DIPA (0.8 ml) via a syringe needle. After the reaction was stirred at 60 °C for 40 h, chloroform and water were then added to the reaction. The organic layer was washed with ammonium hydroxide and dried over anhydrous sodium sulfate and concentrated to yield the crude product as an orange solid, which was re-dissolved in water and dialyzed



**Scheme 1.** Synthesis of water-soluble PPEs. Conditions: (a) 11-Hydroxy-3,6,9-trioxaundecyl-1-*p*-toluenesulfonate,  $\text{K}_2\text{CO}_3$ , acetone, DMF, reflux, overnight, 50%. (b)  $\text{Me}_3\text{SiC}\equiv\text{CH}$  (TMSA),  $\text{Pd}(\text{PPh}_3)_2\text{Cl}_2$ , CuI, *i*-Pr<sub>2</sub>NH (DIPA), toluene, 60 °C, 22 h, 96%. (c) KOH, MeOH-THF, 25 °C, 48 h, 83%. (d)  $\text{Pd}(\text{PPh}_3)_4$ , CuI, *i*-Pr<sub>2</sub>NH, Toluene, 60 h, 91%.

against deionized water for 24 h (500 ml water each for 4 times in a day) to yield an orange solid (98.5 mg, 91%) after dried under vacuum.  $^1\text{H}$  NMR (300 MHz,  $\text{CDCl}_3$ ):  $\delta$  2.09 (s, 2H), 3.56–3.68 (br, m, 20H), 3.79 (br, s, 4H), 3.93 (br, s, 4H), 4.25 (br, s, 4H), 7.08 (s, 2H). GPC (eluent: THF):  $M_n = 9.6$  KD, PDI = 1.8.

## 2.4. PPE/SWNTs Hybrid Synthesis

SWNTs were purified using a previously published method.<sup>20</sup> A typical procedure for the fabrication of hybrid of SWNTs with the PPE is as follows: 2.4 mg purified SWNTs were sonicated in 10 ml distilled water for 2 h to give an unstable suspension of visible insoluble solids. 10 ml PPE water solution (0.3 mg/ml) was then added. The resulting solution was further sonicated for 5 min and then stirred for 3 days at room temperature to give a black-green colored stable clear solution. The sample was then ultracentrifuged for 90 min at 14000 rpm. The sediments were washed with distilled water by six sonication-centrifugation (14000 rpm) cycles in order to remove all the free PPEs to generate the desired hybrid PPE/SWNTs. The PPE concentration in the upper layer was measured using a standard PPE concentration curve generated using the UV-Vis spectra from a series of PPE solution with different concentrations, which was also used later to estimate the PPE/SWNTs ratio in the hybrid (see below). To prepare the hybrid PPE/SWNTs solutions, the PPE/SWNTs hybrid from 2.4 mg purified SWNTs above, was re-dispersed in 10 ml distilled water to form a clear and stable hybrid solution with SWNTs concentration of 0.24 mg/ml. 8 ml of this hybrid solution was diluted to a series of different concentrations for SWNT standard curve measurements and other spectrum measurements (see below). 1 ml this hybrid solution was blended with 5 ml PPE water solution (5 mg/ml) and used for photovoltaic cell fabrication. The mass ratio of SWNTs/PPE for the photoactive layer was  $\sim 1:100$ .

## 2.5. Solubility Measurement

The solubility of SWNTs was measured as follows. The PPE/SWNTs hybrid solution prepared above was divided into several portions and diluted to different concentrations as standard solutions (0.12, 0.09, 0.06, 0.03, and 0.012 mg/ml SWNTs, respectively) and their UV-Vis-NIR absorption spectra were measured. Then, a standard curve of concentration-absorbance dependence at 1020 nm ( $S_{22}$  band from the second pair of singularities in the density of states of the semiconducting SWNTs) was obtained. To measure the solubility of the hybrid PPE/SWNTs, a saturated solution of PPE/SWNTs hybrid was prepared by dissolve 10 mg of PPE/SWNTs hybrid in 2 ml distilled water and was allowed to stand overnight at room temperature. The upper clear layer was carefully taken with a syringe

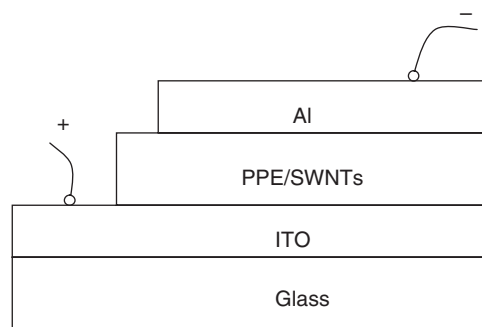


**Fig. 2.** The device architecture view of ITO/PPE-SWNTs/Al photovoltaic cell.

and diluted to a proper concentration where the absorption is in the range of the standard plot. The solubility of SWNTs from the PPE/SWNTs hybrid was determined to be 1.8 mg/ml for the hybrid in water (also see Results and Discussion below).

## 2.6. Photovoltaic Cell Fabrication

Photovoltaic devices were fabricated in the ITO/PPE-SWNTs/Al configuration as shown in Figure 2. The ITO glass ( $2.5 \times 2.5$  cm<sup>2</sup>) was cleaned by ultrasonication and rinsed in deionized water, acetone, and *iso*-propanol. The photoactive layer PPE/SWNTs was prepared using the PPE/SWNTs solution prepared according to the last section and deposited on ITO electrode by spin coating at 1000 rpm and dried at 45 °C under vacuum for 1 h. Al electrode was deposited on the active layer by vacuum evaporation under  $3 \times 10^{-4}$  Pa and the thickness of which was controlled at  $\sim 100$  nm. Eight polymer solar cell devices were fabricated in one cut ITO glass, and the effective area of each cell is 4 mm<sup>2</sup>.

## 3. RESULTS AND DISCUSSION

### 3.1. Synthesis and Characterization of PPE

As shown in Scheme 1, the oligoethyleneglycol-substituted PPE polymer was prepared via Sonogashira cross-coupling procedures. The oligoethyleneglycol groups were used to enhance its water solubility. GPC analysis of the polymer indicated a reasonable degree of polymerization ( $DP \approx 22$ ) and polydispersity ( $PDI \approx 1.8$ ). The structure is confirmed by  $^1\text{H}$ -NMR as shown in the Experimental section. This PPE is readily soluble not only in a wide range of organic solvents, such as chloroform, methanol and THF, but also in water due to the oligoethyleneglycol side chain. The water solubility of PPEs at room temperature was determined to be 8.7 mg/ml using the standard curve (UV-Vis absorption vs concentration) method.

As it can be seen from Figure 3, the PPE in  $\text{CHCl}_3$  exhibited an intense absorption centered at 428 nm, which

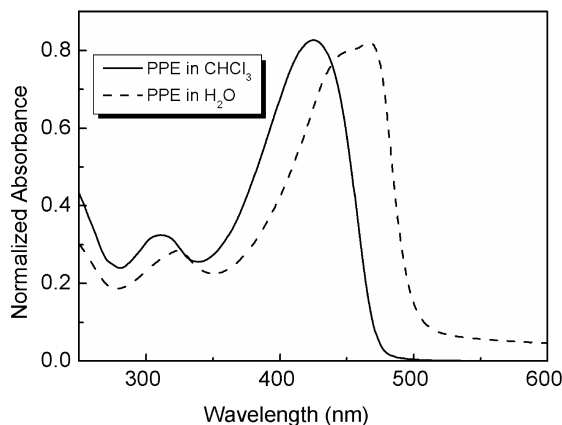


**Fig. 3.** Normalized UV-Vis spectra for PPE in  $\text{CHCl}_3$  and in water.

arises from the long axis polarized  $\pi-\pi^*$  transition corresponding to the effective conjugation along the PPE backbone.<sup>7</sup> When the PPE is dissolved in water, its absorption peak undergoes a 39 nm red shift and becomes broadened, which indicates that in water the PPE intends to exist in a more-aggregated state.<sup>21,22</sup> This conclusion can also be revealed by its fluorescence measurements. As shown in Figure 4, in chloroform the fluorescence appears as a narrow band at 472 nm, which is a typical PPEs emission structure. This suggests that the polymer exists in a monomeric or less aggregated state in chloroform. However, in water, the fluorescence broadens significantly with an “excimer-like” band appearing at 518 nm. Furthermore, a significant 46 nm red shift of the fluorescence peak band is observed in water compared with that in chloroform. In general, the very broad, less efficient and strong red-shift fluorescence is characteristic of conjugated polymer aggregates.<sup>21,22</sup> Though the PPE is soluble in water, the hydrophobic effect and strongly intermolecular  $\pi-\pi$  stacking of the backbone still causes the PPEs to form aggregates in water. The similar reason may also be

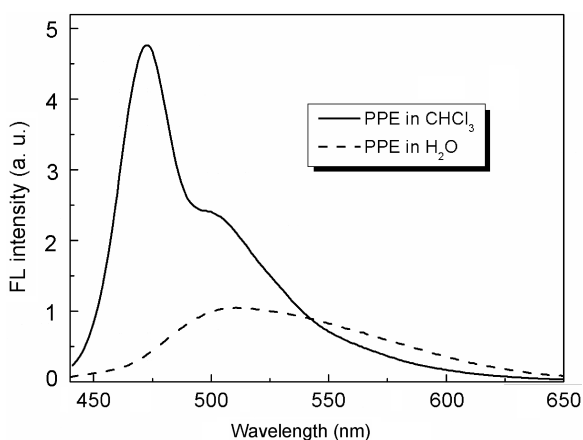


**Fig. 4.** Fluorescence spectra for PPE in  $\text{CHCl}_3$  (0.01 mg/ml) and in water (0.02 mg/ml).

responsible for the strongly interaction between PPEs and SWNTs for the formation of the hybrid discussed below.

## 3.2. Preparation and Characterization of PPE/SWNTs Hybrid

### 3.2.1. Preparation of PPE/SWNTs Hybrid and the SWNT Solubility

Covalent and non-covalent (supramolecular) approaches have been used to functionalize carbon nanotubes to improve their solubility.<sup>23–25</sup> And non-covalent approach is especially desired to modify the nanotube because this strategy preserves the electronic and structural integrity of SWNTs rather than covalent modification, which could damage the continuous  $\pi$ -system of CNTs.<sup>24,26</sup> The good solubility of the PPE and its  $\pi-\pi$  conjugation structure should make it to form stable  $\pi-\pi$  stacking structure with SWNTs and thus enhance the solubility of SWNTs (Fig. 1).

Solution-phase UV-Vis-NIR spectroscopy has been reported to demonstrate a linear relationship between the absorbance and the relative concentrations of SWNTs in different solvents, and has been used to determine the solubility of SWNTs.<sup>16,27</sup> The enhanced solubility of SWNTs from hybrid PPE/SWNTs was measured by UV-Vis-NIR using a standard plot generated from with a series of different concentrations (0.12, 0.09, 0.06, 0.03, and 0.012 mg/ml SWNTs, respectively) as described above. The standard curve of absorption versus concentration was shown in Figure 5 and the absorption values at  $\sim 1020$  nm were plotted against concentrations (in  $\text{mg ml}^{-1}$ , the inset of Fig. 5). This band from SWNTs has been known to be less sensitive to the chemical modification.<sup>28</sup> The upper layer saturated PPE/SWNTs clear solution, prepared by dissolving 10 mg of PPE/SWNTs hybrid in 2 ml distilled

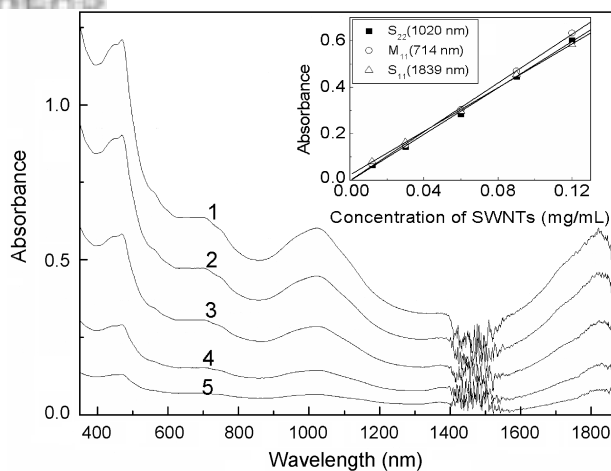


**Fig. 5.** UV-Vis-NIR spectra of PPE/SWNTs hybrid in water (the concentrations of SWNTs are 0.12, 0.09, 0.06, 0.03, and 0.012 mg/ml, respectively). The inset is the plot of absorbance ( $M_{11}$ ,  $S_{11}$ , and  $S_{22}$ ) versus concentration for PPE/SWNTs standard solutions.

water, was diluted to a proper concentration and then used to measure the solubility of SWNTs against the plot in Figure 5. On the basis of the applicability of Beer's law, we can estimate the solubility of SWNTs and it reaches 1.8 mg/ml for the hybrid by measurement of the intensity of the  $S_{22}$  of the diluted hybrid solution. This high solubility provides the possibility to easily disperse SWNTs homogeneously, which allows us to fabricate PPE/SWNTs hybrid and study their properties.

The mass ratio ( $R_m$ ) of PPEs:SWNTs in hybrid, could be calculated from the amount of PPE hybridizing with SWNTs and the amount of the SWNTs in the hybrid. The amount of PPE in the hybrid was the difference of the PPE totally used and that left in the upper layer clear solution from the preparation of the hybrid. The value of  $R_m$  was then calculated using the following equation:

$$R_m = (C_0V_0 - C_1V_1)/W \quad (1)$$

where  $C_0$  is the initial PPE concentration (mg/ml),  $V_0$  is the volume of initial PPE solution,  $C_1$  is the PPE concentration (mg/ml) of the combined centrifugation upper layer solution after interacting with SWNTs,  $V_1$  is the total volume of the centrifugation upper layer solution, and  $W$  is the weight of SWNTs (mg). The mass ratio of PPEs:SWNTs in hybrid thus was estimated as  $R_m = 0.56$ . Thus, significant amount of PPEs stacking on the SWNTs surface guarantees the high solubility and stability of PPE/SWNTs hybrid dispersed in water. This ratio is also quite similar with that reported earlier for the other PPE/SWNTs hybrid.<sup>6</sup>

From Figure 5, the hybrid absorption at different concentration at all the three major peaks from SWNTs including at 714 nm (the  $M_{11}$  band of SWNTs) and 1839 nm (the  $S_{11}$  band of SWNTs) were found to have a linear relationship against concentrations, indicating no light scattering effects occurred. Light scattering effects always bring upward deviation from the linear relationship because the relatively larger SWNTs bundles correspond to stronger scatters.<sup>29</sup> All the linear dependences of absorbance on concentration at different wavelengths support that SWNTs have formed a stable and irreversibly bound complex rather than a simple mixture, which have been homogeneously dispersed in solvents. On the basis of the applicability of Lambert-Beer's law, we can estimate the aqueous effective extinction coefficient of SWNTs in hybrid from the slope of the liner function to be  $9.93 \text{ L g}^{-1} \text{ cm}^{-1}$  at 1020 nm with  $R$  value of 0.999. This result is comparable to previous reports on covalent functionalized SWNTs.<sup>30, 31</sup>

### 3.2.2. Microscopy Analysis and Absorption Studies

The enhanced solubility of SWNTs must come due to the strong interaction of SWNTs with the PPE (Fig. 1),<sup>6</sup> which itself has a good solubility in water. Transmission

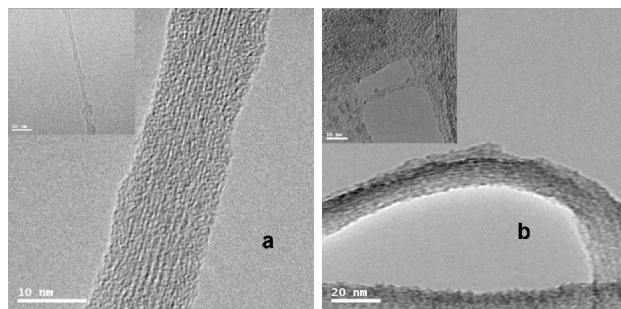


**Fig. 6.** TEM images of SWNTs (a) before and (b) after PPEs functionalization. The insets show the individual SWNTs.

electron microscope (TEM) was allowed to directly image SWNTs samples at the level of individual SWNTs or the thin bundles. Figure 6 shows a typical surface morphology of SWNTs before and after the PPE functionalization. The relative clear and smooth SWNTs surface becomes bumpy after PPE attachment. The inset images of Figure 6 show the individual SWNTs before and after forming the hybrid. Clearly, the sidewall of the SWNTs was significantly roughened by the coverage of soft materials, indicating the non-covalent stacking of PPEs on the surface of SWNTs.

The non-covalent stacking of PPEs on SWNTs is also consistent with the difference in UV-Vis-NIR spectra for their water solutions before and after the functionalization as shown in Figure 7. The spectrum of PPEs is characterized by the typical absorption bands in the 400 ~ 500 nm wavelength region. UV-Vis-NIR spectrtrum for the PPE in the PPE/SWNTs does not have significant change from that for the free PPE, indicating that the  $\pi$ -conjugation of the PPE is largely unchanged. If the polymer wrapped on the nanotube, one would expect a blue shift of the PPE's lowest energy absorption band because of interruption of the  $\pi$ -conjugation. However, after hybridization the absorption

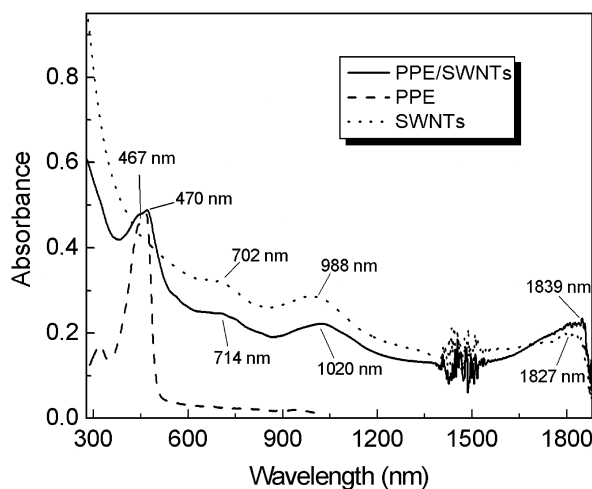


**Fig. 7.** UV-vis-NIR spectra of PPEs (0.02 mg/ml), SWNTs (0.05 mg/ml), and PPE/SWNTs (0.05 mg/ml) hybrid in water.

band of PPEs does show a small red-shift (from 467 nm to 470 nm) and becomes broader. This could be attributed to the stacking of PPEs on the SWNTs surface, which induces slightly better coplanarization of the adjacent phenyl rings in the polymer chain. It is known that there is no steric barrier to rotation of the triple bond links in the PPE polymer structure, which allows the phenyl units in the polymer chain to adopt a better coplanarization on SWNTs.<sup>32</sup> The major features of UV-Vis-NIR absorption for SWNTs were largely unchanged in the hybrid too. The retention of these spectral features in PPE/SWNTs could be considered as the character of non-covalent modification of SWNTs, indicating the electron structure of the nanotube has been preserved. Whereas, we indeed observed some minor changes for SWNTs spectra after the SWNTs are functionalized with PPEs in the hybrid. The characteristic lowest-energy van Hove transitions  $S_{22}$  and  $S_{11}$  of the semiconducting SWNTs near 1000 nm and 1800 nm respectively, and the  $M_{11}$  from the metallic SWNTs near 700 nm did show some shift for the SWNTs in the hybrid:  $S_{22}$  shifts from 988 nm to 1020 nm,  $M_{11}$  shifts from 702 nm to 714 nm, and  $S_{11}$  shifts from 1827 nm to 1839 nm.

The line widths of van Hove transitions are related to the size of SWNTs bundles. Individual, isolated tubes have been reported to give rise to sharp and well-resolved peaks, and SWNTs bundles usually exhibit broad ones.<sup>33</sup> In our case, both naked SWNTs and SWNTs in hybrid exhibit broad peaks, suggesting the bundle state for most SWNTs in water solution. While more individual SWNTs were observed, AFM examination shown in Figure 8 also reveals that SWNTs bundles still dominate PPE/SWNTs system rather than individual SWNTs, which is in accordance with the unresolved fine features for the UV-Vis-NIR absorption spectra of PPE/SWNTs. The Raman spectra (not shown) of SWNTs did not show significant change before and after the functionalization.

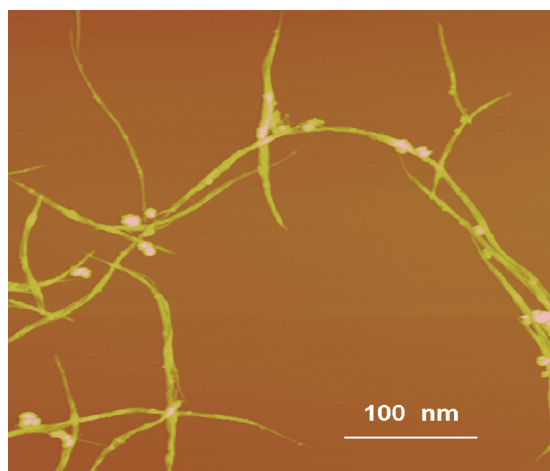


**Fig. 8.** A typical tapping mode AFM image of PPE/SWNTs hybrid. Samples were prepared by dropping its solution on a mica surface and then dried under IR light.

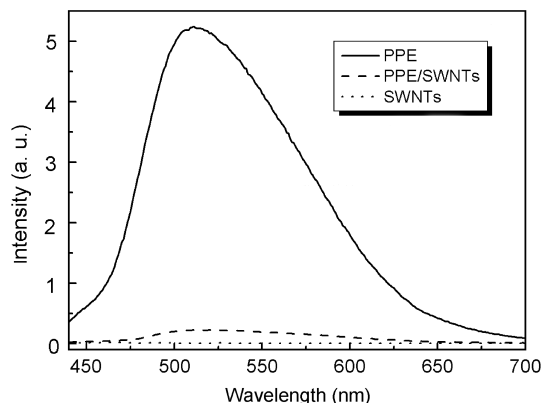


**Fig. 9.** Steady-state fluorescence of PPE (0.01 mg/ml), PPE/SWNTs hybrid (0.028 mg/ml) and SWNTs (0.02 mg/ml) water solutions at  $\lambda_{\text{ex}} = 420$  nm (with equivalent absorbance for free PPE and PPE in the hybrid).

### 3.2.3. Fluorescence Studies

The fluorescence studies also support a significant  $\pi$ - $\pi$  interaction between the polymer and the nanotube (Fig. 9). Upon excitation at 420 nm, the PPE in PPE/SWNTs exhibited >95% fluorescence quenching after subtracting the absorption of SWNTs as compared with that of the free PPE water solution. The quenching likely arises from efficient energy transfer between PPEs and SWNTs via the electron transfer mechanism,<sup>4,16,17</sup> rather than the disruption of  $\pi$ -conjugation caused by a conformational change. Energy transfer quenching between molecules and SWNTs is well known.<sup>34,35</sup> Combined with that from the UV-Vis-NIR studies above, these results clearly support a significant interaction between PPEs and SWNTs with the mode of flat  $\pi$ - $\pi$  stacking in the hybrid, where both the intrinsic structural and electric properties of both PPEs and SWNTs are largely preserved.<sup>6</sup>

The efficient energy transfer between PPEs and SWNTs in the hybrid is also confirmed from the study for the fluorescence lifetimes (Fig. 10) of the hybrid and the free PPE as a reference in water solution. Both the fluorescence

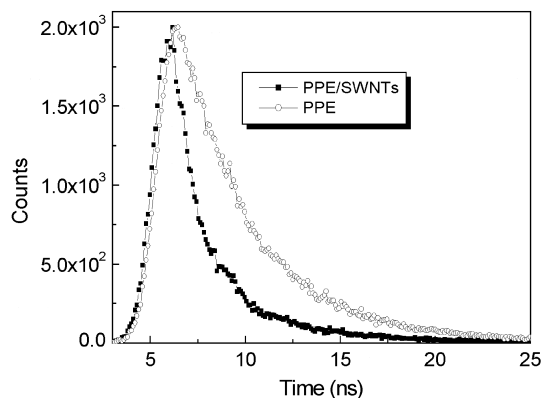


**Fig. 10.** Fluorescence decay curves of PPEs and PPE/SWNTs water solutions at room temperature,  $\lambda_{\text{ex}} = 460$  nm and  $\lambda_{\text{em}} = 510$  nm,  $\chi^2 = 1.30$  and 1.39 for the PPE and PPE/SWNTs, respectively.

traces could be fitted to a double-exponential decay function:<sup>36</sup>

$$I(t) = A_1 \exp(-t/\tau_1) + A_2 \exp(-t/\tau_2) \quad (2)$$

where  $A_1$  and  $A_2$  are preexponential, which correspond to the initial separate fluorescence amplitudes.  $\tau_1$  and  $\tau_2$  are the corresponding fluorescence lifetimes. The resulting short and long lifetimes of free PPEs are  $\tau_1 = 1.4$  ns and  $\tau_2 = 4.4$  ns, with preexponential factors  $A_1 = 5.01 \times 10^{-2}$  and  $A_2 = 4.17 \times 10^{-2}$ , respectively. The average lifetime (2.8 ns) of the decay is calculated from  $\tau_{\text{ave}} = (A_1\tau_1 + A_2\tau_2)/(A_1 + A_2)$ . The fluorescence short and long component lifetimes of PPEs in the hybrid are 0.54 and 3.7 ns, with preexponential factors  $A_1 = 0.16$  and  $A_2 = 1.74 \times 10^{-2}$ , and the average lifetime is  $\tau_{\text{ave}} = 0.84$  ns, significantly smaller compared with 2.8 ns for the free PPE. Thus, after the PPE interacts with carbon nanotubes to form the hybrid, the PPE fluorescence decay becomes significantly faster. This much better efficient energy transfer in the hybrid due to SWNTs implies it could act as a promising photovoltaic material.

According to these time resolved emission results, the average rate of energy transfer can be calculated from the equation:<sup>37</sup>

$$k_{\text{en}} = 1/\tau - 1/\tau_{\text{ref}} \quad (3)$$

where  $\tau$  and  $\tau_{\text{ref}}$  represent the average excited-state lifetime (0.84 ns) of the hybrid and the average lifetime (2.8 ns) of the reference free PPE, respectively. The average rate constant for the energy transfer process from PPEs to SWNTs thus result in  $k_{\text{en}} = 8.3 \times 10^8 \text{ s}^{-1}$ . This value is comparable with that for functionalized  $\text{C}_{60}$  by zinc porphyrin.<sup>38</sup>

### 3.3. Light Energy Conversion

PPEs have been known for their photo-activity in PV applications.<sup>8–10</sup> Considering the existence of efficient energy transfer between PPE and SWNTs and an intrinsic bulk heterojunction structure of our hybrid material, we thus fabricated a photovoltaic device using this material (Fig. 2).

The current–voltage  $I$ – $V$  characteristics of the ITO/PPE-SWNTs/Al devices in dark and under white light illumination (AM 1.5, 100  $\text{mW}/\text{cm}^2$  from the ITO side) are depicted in Figure 11(a). Forward bias is defined as positive voltage applied to the ITO electrode. The dark current is considerably higher in forward bias than in reverse bias, indicating a diode behavior. Under illumination, the hybrid device shows short-circuit current density ( $I_{\text{sc}}$ ) of 28.7  $\mu\text{A}/\text{cm}^2$  and an open-circuit voltage ( $V_{\text{oc}}$ ) of 105 mV (Fig. 12). ITO/PPE/Al devices were also fabricated for a comparison (Fig. 11(b)) which gave a  $V_{\text{oc}} = 0.2$  mV. Its  $I_{\text{sc}}$  was too low to be accurately detected within the measurement limit. Obviously, the addition of SWNTs enhances both the magnitude of  $V_{\text{oc}}$  and  $I_{\text{sc}}$  by  $\sim$  two orders compared to that for

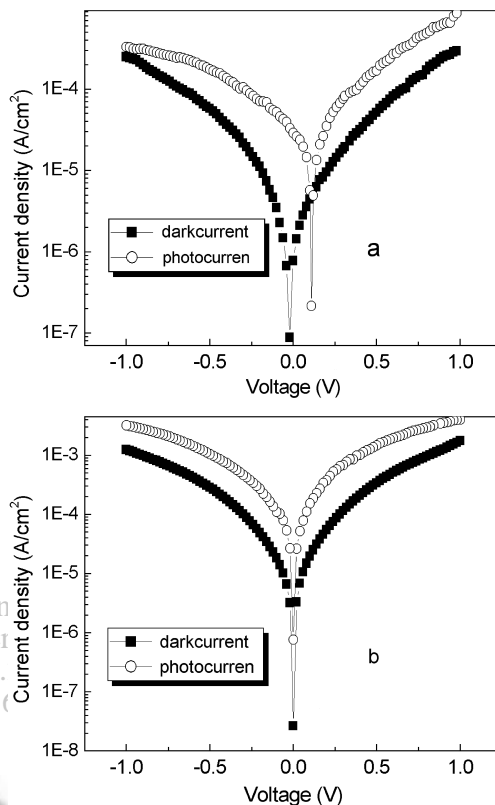


**Fig. 11.**  $I$ – $V$  Characteristics of an ITO/PPE-SWNTs/Al (a) and ITO/PPE/Al (b) devices in dark and under illumination of 100  $\text{mW}/\text{cm}^2$ .

the device using the free PPEs. The much enhancement of photovoltaic properties for the hybrid device is probably due to the introduction of internal polymer/SWNT bulk heterojunction.<sup>12</sup> These junctions act as dissociation centers, which are able to split up the exciton and also create a continuous pathway for charges to be transported to the electrodes.

The magnitude of  $I_{\text{sc}}$  (28.7  $\mu\text{A}/\text{cm}^2$ ) of the hybrid device is comparable with that of other polymer/SWNTs solar cell,<sup>11–13</sup> and about two-fold larger than that (14.5  $\mu\text{A}/\text{cm}^2$ ) using water-soluble polythiophene with SWNTs.<sup>14</sup> While

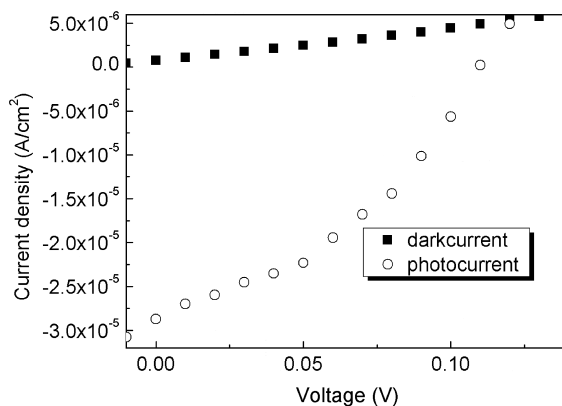


**Fig. 12.**  $I$ – $V$  Characteristics of an ITO/PPE-SWNTs/Al device measured in the dark and under illumination (100  $\text{mW}/\text{cm}^2$ ) as a linear plot.

our open circuit voltage is about 35 times of that of the polythiophene/SWNT device using the water soluble polymer,<sup>14</sup> the absolute magnitude of  $V_{oc}$  (105 mV) is relatively lower compared with other polymer/SWNT PV devices.<sup>11–13</sup> It is known that shunting could cause low  $V_{oc}$  in the heterojunction PV cells using nanotubes.<sup>14</sup> This probably is also the main reason for the low  $V_{oc}$  in our case. Interestingly, the short-circuit current is not affected and still in the normal range. Better film quality may be able to improve the overall PV performance. The enhancement of photovoltaic properties comparing with water-soluble polythiophene/SWNTs device<sup>14</sup> may be contributed to a better bulk heterojunction of PPEs with SWNTs by strong  $\pi$ - $\pi$  stacking and dispersion of SWNTs in water assisted by the PPE through increasing the donor/acceptor interface area.

The fill factor (FF), one of the characteristics which gives the power delivery capability of a photovoltaic cell is calculated by  $FF = (V_m I_m)/(V_{oc} I_{sc})$  to be 0.39, where  $V_m$  and  $I_m$  are the voltage and the current in the maximum power point of the  $I$ - $V$  curve in the fourth quadrant. The power conversion efficiency was calculated from the expression:

$$\eta = \frac{FF \times I_{sc} (\text{A/cm}^2) \times V_{oc} (\text{V})}{P_{in} (\text{W/cm}^2)} \quad (4)$$

where  $V_{oc}$ ,  $I_{sc}$ , FF, and  $P_{in}$  are the open circuit voltage, the short circuit current, the fill factor and the incident light power, respectively. The power conversion efficiency was calculated to be  $1.2 \times 10^{-3}\%$ . Obviously, the hybrid device shows the ability of converting sunlight to electrical power. In the hybrid, the PPE exhibits the property of light harvesting “antenna” and SWNTs here play an important role in better dissociating excitons into electrons and holes and transporting electrons to electrode, which enhance the PV performance.<sup>39</sup> We are currently investigating the PV devices using PPEs modified with low band gap materials that have better IR and NIR absorption to improve the device performance.

#### 4. CONCLUSIONS

In summary, the water-soluble PPE is capable of strongly interacting with SWNTs to form a stable and highly water-soluble PPE/SWNTs nanohybrid. The solubility of SWNTs is significantly enhanced to 1.8 mg/ml. The strong interaction and energy transfer between PPEs and SWNTs are revealed using spectrum analysis such as UV-Vis-NIR and fluorescence spectroscopy. Using this hybrid we have fabricated a photovoltaic device which shows improved photovoltaic performance compared with that without SWNTs. Improving the filming ability and effectively avoiding shunting in the device are expected to enhance the device performance, and further work with better IR and NIR absorption materials is in progress.

**Acknowledgments:** The authors gratefully acknowledge the financial support from MoST (#2006CB0N0700 and 2003AA302640), MoE (#20040055020) and the NSF (#20644004 and 60676051) of China and the NSF (#07JCYBJC03000) of Tianjin City.

#### References and Notes

- H. J. Dai, *Acc. Chem. Res.* 35, 1035 (2002).
- P. M. Ajayan, *Chem. Rev.* 99, 1787 (1999).
- R. H. Baughman, A. A. Zakhidov, and W. A. de Heer, *Science* 297, 787 (2002).
- D. M. Guldi, G. M. A. Rahman, F. Zerbetto, and M. Prato, *Acc. Chem. Res.* 38, 871 (2005).
- H. M. Cheng, *Carbon Nanotube Synthesis, Microstructure, Properties and Applications*, Chemical Industry Press, Beijing (2002).
- J. Chen, H. Y. Liu, W. A. Weimer, M. D. Halls, D. H. Waldeck, and G. C. Walker, *J. Am. Chem. Soc.* 124, 9034 (2002).
- U. H. F. Bunz, *Chem. Rev.* 100, 1605 (2000).
- S. L. Lu, M. J. Yang, J. Luo, and Y. Cao, *Synth. Metal.* 140, 199 (2004).
- J. K. Mwaaura, M. R. Pinto, D. Witker, N. Ananthakrishnan, K. S. Schanze, and J. R. Reynolds, *Langmuir* 21, 10119 (2005).
- A. G. Umnov and O. J. Korovyanko, *Appl. Phys. Lett.* 87, 113506 (2005).
- S. Bhattacharyya, E. Kymakis, and G. A. J. Amaratunga, *Chem. Mater.* 16, 4819 (2004).
- E. Kymakis and G. A. J. Amaratunga, *Appl. Phys. Lett.* 80, 112 (2002).
- E. Kymakis, I. Alexandrou, and G. A. J. Amaratunga, *J. Appl. Phys.* 93, 1764 (2003).
- J. A. Rud, L. S. Lovell, J. W. Senn, Q. Q. Qiao, and J. T. Mcleskey, *J. Mater. Sci.* 40, 1455 (2005).
- B. J. Landi, R. P. Ruffaella, S. L. Castro, and S. G. Bailey, *Prog. Photovolt: Res. Appl.* 13, 165 (2005).
- Z. Guo, F. Du, D. M. Ren, Y. S. Chen, J. Y. Zheng, Z. B. Liu, and J. G. Tian, *J. Mater. Chem.* 16, 3021 (2006).
- D. M. Ren, Z. Guo, F. Du, J. Y. Zheng, and Y. S. Chen, *J. Nanosci. Nanotechnol.* 7, 1539 (2007).
- X. Lv, F. Du, Y. F. Ma, Q. Wu, and Y. S. Chen, *Carbon* 43, 2020 (2005).
- D. C. Lee, B. J. Chang, G. M. Morales, Y. A. Jang, M. K. Ng, S. T. Heller, and L. P. Yu, *Macromolecules* 37, 1849 (2004).
- J. Liu, A. G. Rinzler, H. J. Dai, J. H. Hafner, R. K. Bradley, P. J. Boul, A. Lu, T. Iverson, K. Shelimov, C. B. Huffman, F. Rodriguez-Macias, Y. S. Shon, T. R. Lee, D. T. Colbert, and R. E. Smalley, *Science* 280, 1253 (1998).
- M. R. Pinto, B. M. Kristal, and K. S. Schanze, *Langmuir* 19, 6523 (2003).
- C. Y. Tan, M. R. Pinto, and K. S. Schanze, *Chem. Commun.* 446 (2002).
- Y. Chen, R. C. Haddon, S. Fang, A. M. Rao, P. C. Eklund, W. H. Lee, E. C. Dickey, E. A. Grulke, J. C. Pendergrass, A. Chavan, B. E. Haley, and R. E. Smalley, *J. Mater. Res.* 13, 2423 (1998).
- S. Banerjee, T. Hemraj-Benny, and S. S. Wong, *Adv. Mater.* 17, 17 (2005).
- A. Hirsch, *Angew. Chem. Int. Ed.* 41, 1853 (2002).
- Y. P. Sun, K. F. Fu, Y. Lin, and W. J. Huang, *Acc. Chem. Res.* 35, 1096 (2002).
- B. Zhao, H. Hu, A. P. Yu, D. Perea, and R. C. Haddon, *J. Am. Chem. Soc.* 127, 8197 (2005).
- M. E. Itkis, D. E. Perea, R. Jung, S. Niyogi, and R. C. Haddon, *J. Am. Chem. Soc.* 127, 3439 (2005).
- B. Zhou, Y. Lin, H. P. Li, W. J. Huang, J. W. Connell, L. F. Allard, and Y. P. Sun, *J. Phys. Chem. B* 107, 13588 (2003).

30. B. Zhao, M. E. Itkis, S. Niyogi, H. Hu, J. Zhang, and R. C. Haddon, *J. Phys. Chem. B* 108, 8136 (2004).
31. B. Zhao, M. E. Itkis, S. Niyogi, H. Hu, D. E. Perea, and R. C. Haddon, *J. Nanosci. Nanotechnol.* 4, 995 (2004).
32. F. Y. Cheng and A. Adronov, *Chem. Eur. J.* 12, 5053 (2006).
33. M. J. O'Connell, S. M. Bachilo, C. B. Huffman, V. C. Moore, M. S. Strano, E. H. Haroz, K. L. Rialon, P. J. Boul, W. H. Noon, C. Kittrell, J. P. Ma, R. H. Hauge, R. B. Weisman, and R. E. Smalley, *Science* 297, 593 (2002).
34. R. B. Martin, L. W. Qu, Y. Lin, B. A. Harruff, C. E. Bunker, J. R. Gord, L. F. Allard, and Y. P. Sun, *J. Phys. Chem. B* 108, 11447 (2004).
35. M. Alvaro, P. Atienzar, P. la Cruz, J. L. Delgado, V. Troiani, H. Garcia, F. Langa, A. Palkar, and L. Echegoyen, *J. Am. Chem. Soc.* 128, 6626 (2006).
36. M. Moffitt, J. P. S. Farinha, M. A. Winnik, U. Rohr, and K. Mullen, *Macromolecules* 32, 4895 (1999).
37. A. Sautter, B. K. Kaletas, D. G. Schmid, R. Dobrawa, M. Zimine, G. Jung, I. H. M. van Stokkum, L. De Cola, R. M. Williams, and F. Würthner, *J. Am. Chem. Soc.* 127, 6719 (2005).
38. A. S. D. Sandanayaka, K. Ikeshita, Y. Araki, N. Kihara, Y. Furusho, T. Takata, and O. Ito, *J. Mater. Chem.* 15, 2276 (2005).
39. J. X. Geng and T. Y. Zeng, *J. Am. Chem. Soc.* 128, 16827 (2006).

Received: 4 April 2007. Revised/Accepted: 10 April 2007.

Delivered by Ingenta to:  
McMaster University  
IP : 130.113.111.210  
Tue, 24 May 2011 16:50:01

